

## Measurement of the Daily Interplanetary Magnetic Field Using the Cosmic-ray Sun Shadow by LHAASO-KM2A.

Yuncheng Nan,<sup>a,\*</sup> , Songzhan Chen<sup>a</sup> and , Cunfeng Feng<sup>b</sup> for the LHAASO Collaboration

<sup>a</sup>Key Laboratory of Particle Astrophysics, Institute of High Energy Physics, CAS, 19B, Yuquan Road, Shijingshan District, Beijing, China

<sup>b</sup>Shandong University, Institute of Frontier and Interdisciplinary Science, 72, Binhai Road, Jimo, Qingdao, Shandong, China

E-mail: [nanyc@ihep.ac.cn](mailto:nanyc@ihep.ac.cn)

The interplanetary magnetic field(IMF) between the Sun and the Earth induces the displacement of the cosmic-ray Sun shadow from the optical position. LHAASO is a large hybrid extensive air shower (EAS) array at Haizi Mountain, 4410 m a.s.l., in China. It is composed of three sub-arrays. The one square kilometer array of LHAASO operated since the end of 2019 and denoted as LHAASO-KM2A, can observe the Sun shadow with a daily significance exceeding 5 standard deviations which is crucial to monitor the variation of its displacement. Using the daily Sun shadow observation achieved by LHAASO-KM2A at the energy  $\sim 40$  TeV and the IMF measurement achieved by OMNI at 1AU in 2021, we found that there was a good cross correlation between them while the variation of the former was  $\sim 3$  days earlier than that of the latter on average. This made it possible, for the first time, to measure the daily  $B_y$  of the IMF reaching 1 AU position in advance with the daily monitoring of the Sun shadow. In addition, combined with the simulation, the time advance is found to be related to the spiral structure of the IMF and its different observation positions. This implies the possibility of using time advance to diagnose Parker's model in the future.

38th International Cosmic Ray Conference (ICRC2023)  
26 July - 3 August, 2023  
Nagoya, Japan



\*Speaker

## 1. Introduction

The interplanetary magnetic field(IMF) which is derived from the coronal magnetic field blown out by the radial solar wind and twisted by the Sun's rotation, is a spiral structure in the solar equatorial plane according to Parker's model[1]. Taking a solar wind speed of  $400 \text{ km s}^{-1}$ , the spiral angle between the IMF and radial direction at 1 AU is  $\sim 45^\circ$ . Early spacecraft confirmed these on average[2]. The deviation between the observed and Parker's spiral angle in the past are related to and promote the study of the systematic changes, the coronal mass ejection(CME), the stream interaction region(SIR) and other disturbances with time scale are far less than 1 solar rotation in the IMF.

Among them, the deviation between the observed and Parker's spiral angle in the static state is the most basic and still unknown problem, although the apparent deviation has been continuously observed over the past few decades. In addition, the effect of different distances from the Sun on deviation has not been discussed because it is difficult to capture the overall deviation in the Sun-Earth connection in situ spacecraft.

The Sun shadow, which is formed by the Sun casting charged cosmic rays from outside the solar system and reach to the Earth, can carry the information about the IMF in the Sun-Earth space[3]. Tibet AS $\gamma$  experiment directly observed the influence of the IMF on the displacement of the Sun shadow[4]. Then, the ARGO-YBJ experiment used the displacement of the Sun shadow in the north-south direction to quantitatively measure the mean y component of the IMF,  $B_y$ , at 1 AU in each solar rotation by folding the data for years of solar activity minimum and prospectively estimated for  $\sim 2$  days in advance in the observed time compared with that measured by spacecraft at 1 AU, as a function of forecast[5]. However, due to the limited observational sensitivity, the forecast has not been realized.

The Square Kilometre Array (KM2A), as one of the main ground arrays in the large high altitude air shower observatory(LHAASO), is expected to observe the Sun shadow with a significance of exceeding  $-5 \sigma$  in 2 days when ignoring the influence of magnetic fields[6]. With this high observational sensitivity, the measurement of the  $B_y$  at the day scale by Sun shadow in advance can be realized. And the time advance including the IMF's information from the integration along the Sun-Earth connection by the Sun shadow, and from the spacecraft at 1 AU, may be used to diagnose Parker's model.

In this work, we present the time advance and the correlation result between the displacement of the Sun shadow in the north-south direction and  $B_y$  through correlation analysis methods to show the possibility of the measurement of the daily  $B_y$  of the IMF reaching 1 AU position in advance by LHAASO. Combining with the simulation of the Sun shadow, we explained the time advance contained information on the spiral structure of the IMF, and showed its possible diagnostic ability for Parker's model to describe the static state IMF.

## 2. Experiment and data analysis

LHAASO is a new-generation complex extensive air shower array located at Daocheng(4410 m above sea level) in the Sichuan province of China[7, 8]. The KM2A in LHAASO contains 5216 electromagnetic particle detectors (EDs) and 1188 muon detectors (MDs), and one of its objectives is to measure charged Cosmic ray above 10TeV. The 1/2-KM2A, including 2365 EDs and 578 MDs, 3/4-KM2A, including 3978 EDs and 917 MDs, and the full KM2A have been operating since December 2019, December 2020, and July 2021.

In this work, we selected annual data for 2020, 2021 and 2022, in the years of solar activity ascending. The zenith angle of the cosmic ray is less than  $50^\circ$ . The number of fired EDs after filtering with the time window of 150 ns and the space window of 200 m is  $26 \sim 251$ . The corresponding median energy of the cosmic ray is  $\sim 40$  TeV and the angular resolution is  $0.5^\circ$ .

To observe the Sun shadow, a circular window with a radius of  $5^\circ$  centred on the optical site of the Sun in local coordinates is used, called the on-source window. And then the equal zenith angle method[9], concretely, 20 off-source windows of the same size and at the same zenith angle are symmetrically aligned on both sides of the on-source window, is used to estimate its background. To directly observe the influence of the IMF on the Sun shadow, the sky map is divided into  $0.025^\circ \times 0.025^\circ$ (the east-west and north-south directions) grids in the geocentric solar ecliptic (GSE) coordinate system is established. The cosmic ray event map and the corresponding background map are formed according to the direction of the cosmic rays in on and off-source windows, respectively. The signals in each grid are extracted by a smoothing procedure with weight, and the corresponding significance is estimated via the Li&Ma formula(see equation 2.5 in [10]). Then, the displacement of the Sun shadow is calculated via a likelihood ratio test between the one-source model, which includes the displacements along the north-south and west-east directions as free parameters, and the background-only model(see details in [11]).

Then the Sun shadows observed for each year are shown in Fig. 1, respectively. The significance of the Sun shadow in 2021 is the highest, reaching about  $-103 \sigma$ . There is no obvious displacement of the Sun shadow in the north-south direction,  $D$ , can be observed in 2021. Then the  $D$  of the Sun shadows which includes the information of  $B_y$  and observed each day exceeding  $5\sigma$  from March 21 to October 2, 2021 is calculated. The  $B_y$  of each day in the GSE coordinate system is the WIND spacecraft measured at 1AU and collected by OMNI[12].

The same analysis is also applied to the Moon shadow to understand the systematic errors of the measurement and to check the stability between 3/4 and full KM2A. The systematic displacement of the Moon shadow in the north-south direction in the equatorial coordinate system is  $-0^\circ.01 \pm 0^\circ.01$ , the expansion of the Moon shadow, including the angular resolution information, and its east-west displacement, including the energy information, are stable in both arrays. Because the systematic error in the north-south position is very small, it is ignored in subsequent observations of the Sun shadow.

The Discrete Correlation Function (DCF) method[13] is used to check the correlation in time series  $D$  and  $B_y$  which have known measurement errors and different lengths due to

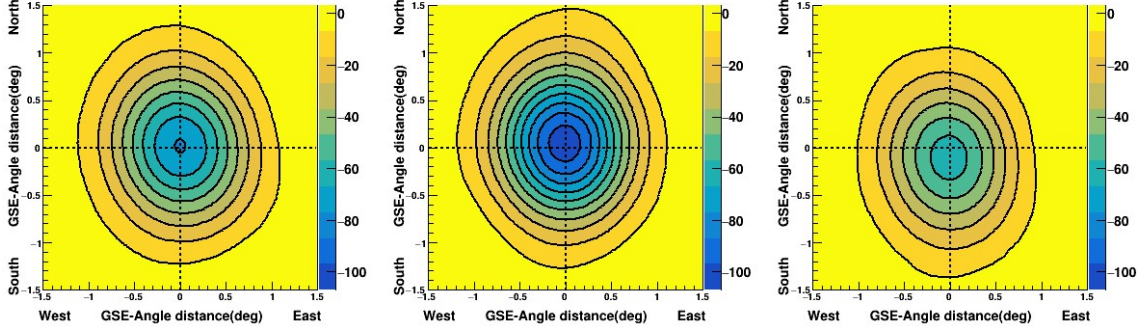


**Figure 1:** The significance maps of the Sun shadows were measured for 2020(left plot), 2021(middle plot) and 2022(right plot), respectively. The central circle of the contour map in 2021 indicates a significance of  $-102.5 \sigma$ , and the step between contour lines is  $10 \sigma$ .

missing measurements sometimes.  $B_y$  is obtained from the mean value of the hourly IMF distribution within 24 hours and the time lag bin width is 0.0625 days. Under different time lag bins, the DCFs between  $D$  and  $B_y$  are calculated. The confidence of the DCF is calculated by the Monte Carlo method as done in [14]. Assuming that the frequency spectrum of the observed  $D$  is a Gaussian random variable,  $10^5$  random  $D$  is generated. Then the DCF is applied with each artificial  $D$  and the observed  $B_y$ . At each time lag bin, a distribution of  $10^5$  DCF is obtained, and we find the most probable by  $3 \sigma$  of the cumulative distribution of the DCF. The time lag with the maximum DCF above the confidence of  $3 \sigma$  is chosen as the result. And corresponding error is calculated by the Monte Carlo method as done in [15].

### 3. Monte Carlo simulation

The Sun shadow simulation is used to interpret the time lag between  $D$  and  $B_y$ . Cosmic rays whose primary chemical composition is obtained mainly from [16] are simulated. The cascade processes within the atmosphere were simulated via the CORSIKA code[17] and then responded in the detector via the G4KM2A code[11, 18]. At the top of the atmosphere, particles with an opposite charge to the cosmic rays are thrown back to around the Sun within the window of  $10^\circ \times 10^\circ$  isotropically. Then we track the paths of the cosmic rays in the Sun-Earth space magnetic field by the relation between the momentum change and the position change according to the momentum theorem, to obtain the particles of the Sun shadow hitting the Sun.

The magnetic fields affect the movement of cosmic rays, including the coronal magnetic field(CMF), the IMF and the geomagnetic field(GMF), are accurately calculated. For the CMF, we use the photospheric magnetograms from GONG[19]("mrnqs" in the file name), and the magnetic field extrapolation model is the Potential Field Source Surface (PFSS)[20], where the source surface ( $R_{ss}$ )= $2.5R_\odot$  with the order of spherical harmonics expansion  $n$  is set to 9. For the GMF, we use the international geomagnetic reference field-13[21] with the order of spherical harmonics expansion  $n$  set to 13 within 600 km above the Earth's surface, and 2 above that.

In Parker's model, the IMF in heliocentric spherical coordinates  $(r, \theta, \phi)$  is given by

$$B = B_r(R_{ss}, \theta, \phi_0) \left(\frac{R_{ss}}{r}\right)^2 \left[ \hat{e}_r - \frac{\omega(r - R_{ss}) \sin \theta}{v} \hat{e}_\phi \right], \quad (1)$$

where  $B_r(R_{ss}, \theta, \phi_0)$  is the initial value at  $R_{ss}$  from the PFSS model and the  $\phi_0$  satisfied the streamline

$$(\phi - \phi_0) \frac{v}{R_{ss} \omega} = \frac{r}{R_{ss}} - 1 - \ln\left(\frac{r}{R_{ss}}\right), \quad (2)$$

where  $v$  is the radial component of the solar wind velocity and  $\omega$  is the angular velocity of the Sun. The spiral angle equals  $\tan^{-1}\left(\frac{B_\phi}{B_r}\right)$ . In this work,  $v$  comes from the daily average observation from OMNI[12] and  $\omega$  is calculated by the rotation period of the Sun ( $\sim 25.4$  days).  $B_r(R_{ss}, \theta, \phi_0)$  is additionally multiplied by 5.7 to make the average daily IMF the same as the observed one.

Using the same analytical conditions and background estimation methods as the observed Sun shadow, we obtained the simulated Sun shadow. More details about the Sun shadow simulation can be found in [22, 23].

#### 4. Results and discussions

The observed  $D$  from LHAASO and the  $B_y$  from OMNI on each day are shown in Fig. 2(a) and (b), respectively. The  $D$  and the  $B_y$  have a similar change trend following time and an obvious time advance can be seen. The correlation analysis between  $D$  and  $B_y$  is calculated. The time lag is obtained as  $3.3 \pm 0.1$  days, and the corresponding DCF exceeds  $3 \sigma$  probable. This verified the correlation and the advance in time between  $D$  and  $B_y$ . Under such a result, after deducting the time advance, the daily observed  $D$  can be used to measure the  $B_y$  that reaches 1AU 3.3 days later.

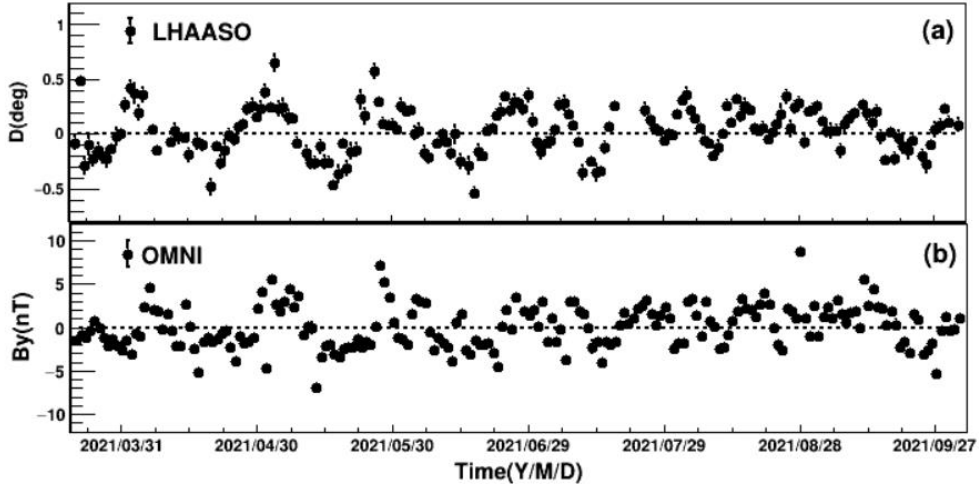


**Figure 2:** Daily variations of (a) the displacement of the Sun shadow in the north and south direction  $D$  and (b) the y component of the IMF  $B_y$  in the GSE coordinate system at 1AU from OMNI. The error bar for  $D$  is the statistical error, and for  $B_y$  is the measurement error.

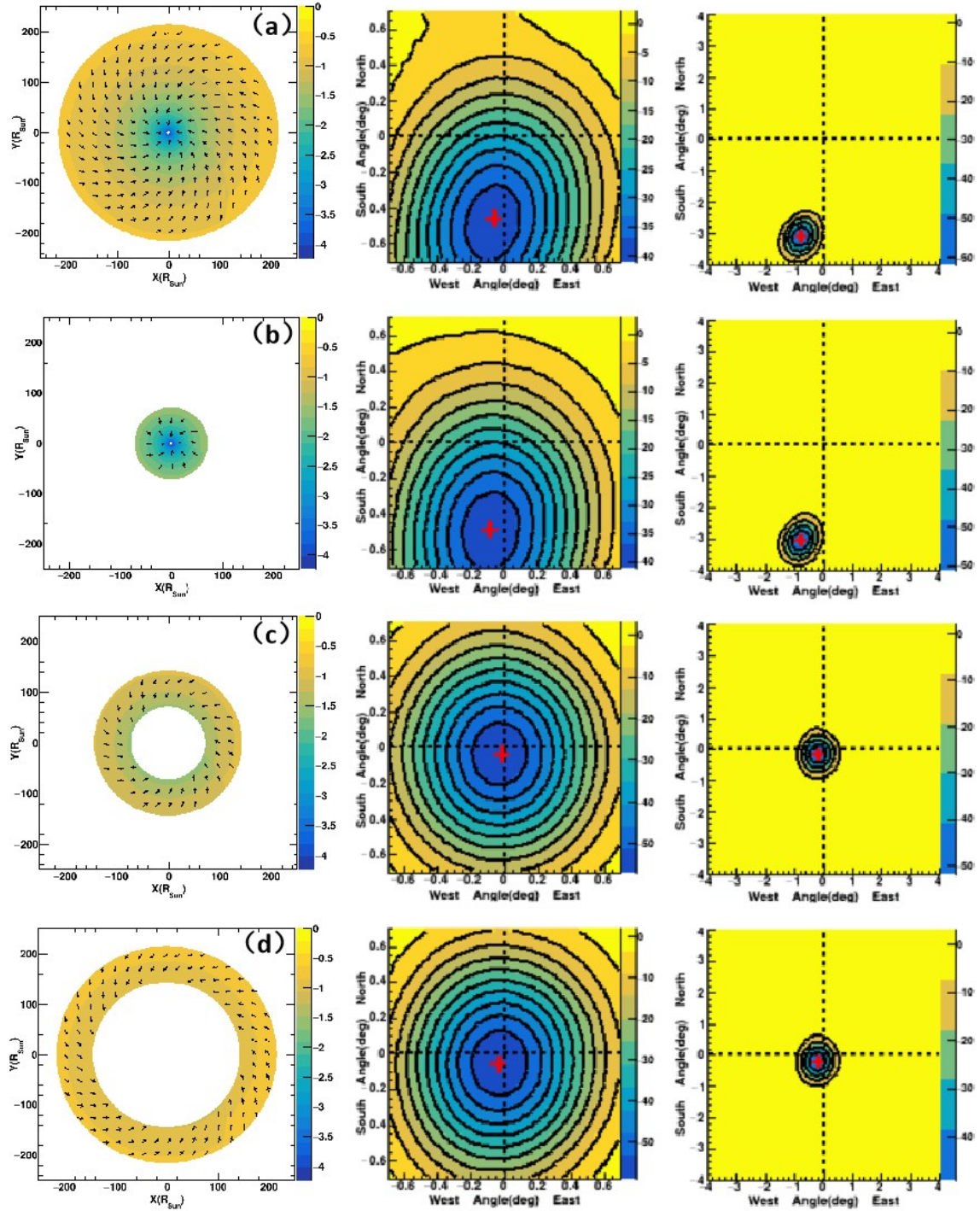


**Figure 3:** IMF (Column 1), simulated Sun shadow with MJD=59381 for LHAASO (Column 2) and for an energy of 5 TeV and a composition of proton only (Column 3). Panels (a), (b), (c) and (d) are the  $\log_{10}$ IMF between  $0 \sim 1$ ,  $0 \sim 1/3$ ,  $1/3 \sim 2/3$ ,  $2/3 \sim 1$  AU in the ecliptic plane around the Sun. The arrows show the direction of the spiral fields. The panels in Columns 2 and 3 are the significance maps of the Sun shadows under the corresponding magnetic fields in the same Row. The central circle of the contour map indicates a minimum significance, and 11 and 5 contours of equal size for Columns 2 and 3, respectively.

Then the formation mechanism of the observed time advance was understood by the Sun shadow simulation. Based on Parker's model in different ranges of Sun-Earth space, the  $D$ s of the Sun shadows with MJD=59381 for LHAASO and for the energy of 5 TeV and composition of proton only are shown in Columns 2 and 3 in Fig. 3, respectively. Based on the total IMF, the  $D$  for LHAASO with an energy of  $\sim 40$ TeV is smaller than that with an energy of 5 TeV and a composition of proton only. It is related to the different energies. Then we found that the  $B_y$  within 1/3 AU near the Sun is responsible for almost total  $D$  of Sun shadow from LHAASO and Sun shadow with an energy of 5 TeV and a composition of proton only. And the effect of the energy on time advance is not significant. Therefore, the average observation position of  $D$  to  $B_y$  is within 1/3 AU on this day. According to Parker's model, the spiral field line may be first detected by the Sun shadow within 1/3 AU and then by spacecraft in 1 AU when frozen inside the wind and moved with Sun's rotation. Considering that the average wind speed  $v$  from OMNI is  $380 \text{ km}^{-1}$ , the IMF will reach 1/3 AU in about 1.5 days and 1 AU in about 4.6 days later from the Sun. The roughly estimated difference in observation time between the above two positions reached about 3 days, which is consistent with the observed time advance. Therefore, the time advance is related to the spiral structure of the IMF and its different observation positions. This implies the possibility of using time advance to diagnose Parker's model in the future.

## 5. Conclusions

Using the daily Sun shadow observation achieved by LHAASO-KM2A at the energy  $\sim 40$  TeV and the IMF measurement achieved by OMNI at 1AU in 2021, we found that there was a good cross correlation between them while the variation of the former was  $\sim 3$  days earlier than that of the latter on average. This made it possible, for the first time, to measure the daily  $B_y$  of the IMF reaching 1 AU position in advance with the daily monitoring of the Sun shadow. In addition, combined with the simulation, the time advance is found to be related to the spiral structure of the IMF and its different observation positions. This implies the possibility of using time advance to diagnose Parker's model in the future.

## 6. Acknowledge

This work is supported by the following grants: The National Key R&D program of China No.2018YFA0404201, No.2018YFA0404202, No.2018YFA0404203, No.2018YFA0404204, National Natural Science Foundation of China No.12022502, No.12205314, No. 12105301, No. 12261160362, No.12105294, No.U1931201, China Postdoctoral Science Foundation No.2022M723150, and in Thailand by the NSRF via the Program Management Unit for Human Resources & Institutional Development, Research and Innovation (No. B37G660015).

## References

- [1] E. N. Parker, *Astrophys. J.* 128, 664 (1958).

- [2] N. F. Ness and J. M. Wilcox, *Phys. Rev. Lett.* 13, 461 (1964).
- [3] G. W. Clark, *Phys. Rev.* 108, 450 (1957).
- [4] M. Amenomori et al. (Tibet AS $\gamma$  Collaboration), *Astrophys. J.* 415, L147 (1993).
- [5] G. Aielli et al. (ARGO-YBJ Collaboration), *Astrophys. J.* 729, 113 (2011).
- [6] S. Wu et al. (LHAASO Collaboration), *Astropart. Phys.* 103, 41 (2018).
- [7] Z. Cao et al. (LHAASO Collaboration), *Chin. Astron. Astrophys.* 43, 457 (2019).
- [8] H. H. He, *Radiat. Detect. Technol. Methods* 2, 7.1 (2018).
- [9] M. Amenomori et al. (Tibet AS $\gamma$  Collaboration), *Phys. Rev. D* 47, 2675 (1993).
- [10] Y. C. Nan and S. Z. Chen, in proceeding of 35th ICRC (2017).
- [11] F. Aharonian et al. (LHAASO Collaboration), *Chin. Phys. C* 45, 025002 (2021).
- [12] NASA OMNI Web Plus, <https://omniweb.gsfc.nasa.gov>.
- [13] R. A. Edelson and J. H. Krolik, *Astrophys. J.* 333, 646 (1988).
- [14] D. R. S. Robertson, L. C. Gallo, A. Zoghbi, and A. C. Fabian, *Mon. Not. R. Astron. Soc.* 453, 3455 (2015).
- [15] S. Xiao et al., *Astrophys. J.* 920, 43 (2021).
- [16] T. K. Gaisser, T. Stanev, and S. Tilav, *Front. Phys.* 8, 748 (2013).
- [17] D. Heck, J. Knapp, J. N. Capdevielle, G. Schatz, and T. Thouw. (1998).
- [18] S. Z. Chen, in proceeding of 36th ICRC (2019).
- [19] GONG Web, <https://gong.nso.edu/>.
- [20] K. H. Schatten, J. M. Wilcox, and N. F. Ness, *Sol. Phys.* 6, 442 (1969).
- [21] P. Alken et al., *Earth Planets Space* 73, 49 (2021).
- [22] Y. C. Nan, C. F. Feng, S. Z. Chen, and C. W. Jiang, in proceeding of 36th ICRC (2019).
- [23] Y. C. Nan, S. Z. Chen, C. F. Feng, and Lhaaso Collaboration, in proceeding of 37th ICRC (2022).